Laser plasma x-ray source for ultrafast time-resolved x-ray absorption spectroscopy

L. Miaja-Avila,[1] G. C. O'Neil,[1] J. Uhlig,[2] C. L. Cromer,[1] M. L. Dowell,[1]
R. Jimenez,[3] A. S. Hoover,[4] K. L. Silverman,[1] and J. N. Ullom[1]
[1]*National Institute of Standards and Technology, Boulder, Colorado 80305, USA*
[2]*Department of Chemical Physics, Lund University, Lund, Sweden*
[3]*JILA, University of Colorado, Boulder, Colorado 80309, USA*
[4]*Los Alamos National Laboratory, Los Alamos, New Mexico 87545, USA*

(Received 2 December 2014; accepted 15 February 2015; published online 2 March 2015)

We describe a laser-driven x-ray plasma source designed for ultrafast x-ray absorption spectroscopy. The source is comprised of a 1 kHz, 20 W, femtosecond pulsed infrared laser and a water target. We present the x-ray spectra as a function of laser energy and pulse duration. Additionally, we investigate the plasma temperature and photon flux as we vary the laser energy. We obtain a 75 μm FWHM x-ray spot size, containing $\sim 10^6$ photons/s, by focusing the produced x-rays with a polycapillary optic. Since the acquisition of x-ray absorption spectra requires the averaging of measurements from $>10^7$ laser pulses, we also present data on the source stability, including single pulse measurements of the x-ray yield and the x-ray spectral shape. In single pulse measurements, the x-ray flux has a measured standard deviation of 8%, where the laser pointing is the main cause of variability. Further, we show that the variability in x-ray spectral shape from single pulses is low, thus justifying the combining of x-rays obtained from different laser pulses into a single spectrum. Finally, we show a static x-ray absorption spectrum of a ferrioxalate solution as detected by a microcalorimeter array. Altogether, our results demonstrate that this water-jet based plasma source is a suitable candidate for laboratory-based time-resolved x-ray absorption spectroscopy experiments.

[http://dx.doi.org/10.1063/1.4913585]

I. INTRODUCTION

The study of the structural dynamics in matter has been enabled by experimental tools such as time-resolved x-ray diffraction and absorption.[1,2] The short wavelength of x-ray light enables materials to be probed at the atomic level and the large penetration depth of hard x-ray light is well suited for the study of crystals, molecules, and protein structures. Consequently, it has recently become possible to measure the dynamic structure of crystalline materials with sub-picosecond and sub-Angstrom resolution using ultrafast x-ray diffraction.[3] However, many chemical and biological processes occur in non-crystalline phases, particularly in liquids. X-ray diffraction of liquids has proven to be challenging because of the lack of long-range order and the presence of the solvent. In contrast, x-ray absorption spectroscopy (XAS) is sensitive to the local structure around element-specific absorption centers. This local structure is preserved in materials without long-range order making XAS an attractive tool for the determination of structures in non-crystalline, liquid, or otherwise disordered systems. Time-resolved XAS can be used to study the pathways of photoactivity in these systems.

Historically, synchrotrons have been one venue for ultrafast XAS studies; these large scale facilities provide hard x-ray pulses with high brilliance and typical durations of 50–100 ps. Pulse durations below 100 fs can be achieved at sliced synchrotron beamlines[4–6] and at emerging x-ray free electron laser facilities.[7] However, the development of laser-driven plasma sources has enabled ultrafast XAS measurements to be performed in laboratory settings.[8–10]

Important characteristics of these table-top x-ray sources relevant for time-resolved XAS are: ultrashort pulse durations, a continuous spectrum from soft to hard x-ray energies, intrinsic all optical and, in principle, jitter-free synchronization with the exciting light source, sufficient photon fluxes, and long-term stability. Many hard x-ray plasma sources rely on focusing high-peak intensity femtosecond laser pulses onto thin metallic targets.[11–16,45] At the high intensities needed for x-ray generation, the metallic target is usually damaged irreversibly. Thus, the continuous generation of x-rays depends on replenishment of the target with each laser pulse, often by rapid spool-to-spool movement of a tape or wire.[14] This replenishment is an engineering challenge since the target must move rapidly with minimal lateral displacement to ensure stable x-ray generation. Furthermore, the local destruction of the target produces debris within the source enclosure that may coat optical elements, reducing transmission of the driving laser and generated x-rays. Thus, some research groups have developed laser-driven x-ray sources based on liquid targets such as distilled water,[17] salt solutions,[18,19] and liquid metals.[20,21] Liquid-target sources have clear benefits for stable, long-term operation: the target is easily replenished and debris can be easily removed from the surfaces of the target enclosure, in some cases by the same pumping action that evacuates the enclosure.

In this manuscript, we describe an x-ray plasma source with a water target designed for ultrafast XAS. We present the measured spectral properties of the x-ray pulses as a function of the laser pulse energy and duration. Since the acquisition of x-ray absorption spectra requires the averaging of measurements from many laser pulses, we also present data on the source stability, including single pulse measurements of the x-ray yield and the x-ray spectral shape. We also show a static x-ray absorption spectrum of a flowing ferrioxalate/water solution taken with this setup. Our results demonstrate that this water-jet based plasma source is a suitable candidate for laboratory-based time-resolved x-ray absorption spectroscopy experiments.

II. EXPERIMENTAL SET-UP

Our experimental set-up (see Fig. 1) is comprised of a high-power ultrafast laser system, a custom-made x-ray generation chamber, an x-ray focusing optic, and two energy-resolving x-ray detectors.

The laser system is a commercial Ti:Sapphire amplifier capable of delivering 800 nm, 35 fs, p-polarized pulses with an energy per pulse of 20 mJ at a repetition rate of 1 kHz. The contrast between the main pulse and pre-pulses in a time window of ± 50 ns was measured to be $>10^4$. This high contrast ratio is necessary to prevent the generation of undesirable high-energy electron beams.[22] A beamsplitter is used to direct approximately 60% of the laser power to the optical path used for x-ray generation. The beam is expanded using a 1:2 telescope, then passed through a half-wave plate and thin polarizer, and is finally focused by a 90° off-axis parabolic mirror with an effective focal length of 100 mm. Because of losses in the optical beam path, the highest pulse energy delivered to the target was 7.8 mJ. The FWHM at the focal spot is measured to be 10 μm, so the average pulse intensity at maximum laser power is 3×10^{17} W/cm^2. The p-polarized focused laser beam interacts at grazing incidence with a water jet in the x-ray generation chamber under a pressure of 7 Torr achieved by evacuating the chamber using a 185 l/min scroll pump. At the interaction region, part of the laser light is reflected by the generated plasma towards the walls of the chamber. As a result, we focus the laser beam on the side of the water jet opposite to the x-ray polycapillary to avoid damaging this valuable piece of apparatus with the reflected optical beam. The remaining 40% of the laser energy is available for photoactivation of samples of interest.

The x-ray generation chamber was constructed from 10 mm thick aluminum with additional 5 mm thick stainless steel shields attached for radiation safety purposes. The chamber has a number of windows for input and output of the laser beam, extraction and assessment of the x-ray photons, and optical alignment of the laser beam and water target. The target consists of a downward flowing water jet created by passing distilled water through plastic tubing lines leading to a thin 100 μm circular aperture. The resulting water jet has a diameter very near 100 μm and a measured speed of $\sim$10 m/s. The water column travels 1 cm between laser pulses, thus renewing the jet surface. No pump is required to supply water to the jet; fluid is drawn into the jet head

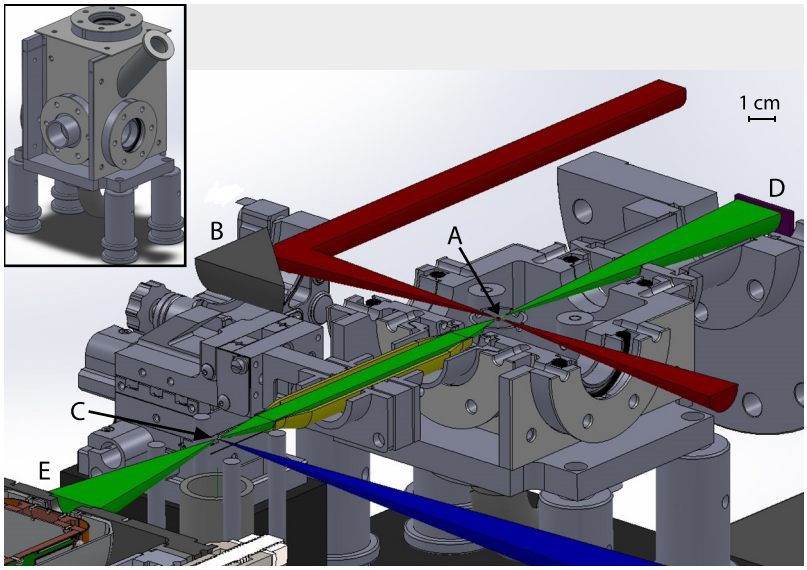

FIG. 1. Experimental setup for time-resolved x-ray absorption spectroscopy. The figure is constructed from three-dimensional machine drawings with a sectioning cut defined by a horizontal plane at the height of the laser and x-ray beams. This cut reveals the interior of the water jet chamber. Laser pulses at 800 nm from a Ti:sapphire amplifier are split into two beams. One beam (red) is tightly focused onto a water jet (A) by a 90° off-axis parabolic mirror (B) with an effective focal length of 100 mm to generate ultrashort x-ray pulses. The resulting x-ray flux is isotropic but x-rays only emerge from the chamber in two beams (green). The second laser beam (blue) is used to photoexcite the sample (C) under study. A CCD camera (D) is used to optimize and monitor the x-ray flux. Opposite to the CCD is a polycapillary x-ray optic (yellow) that collects x-rays from the water jet and focuses them in a 75 μm FWHM circular spot at the sample location. The sample can be optically pumped in a direction perpendicular to the x-ray beam. The x-rays that are transmitted through the sample are analyzed by an array of microcalorimeter detectors (E). The exterior of the water jet chamber is shown in the inset.

by the vacuum conditions inside the chamber. To prevent the formation of ice in the chamber, care was taken to ensure that water from the jet exits into a separate reservoir. We have demonstrated operation of the water jet for hundreds of hours without plugging of the aperture.

The plasma source emits x-rays into a full 4π solid angle. As a result, x-ray optics are sometimes used to collect x-rays from the source and refocus them onto a sample. This is done to physically separate the sample from the source target while maintaining a high x-ray flux at the sample. Unfortunately, some x-ray optics can significantly increase the x-ray pulse duration, thus special care to limit pulse broadening has to be taken into account in the design of these optics. A detailed discussion and comparison of x-ray optics is presented by Bargheer *et al.*[23] and Shymanovich *et al.*[24] In our setup, a polycapillary x-ray optic collects the x-ray photons from the generation chamber and focuses them onto a circular 75 μm FWHM spot 25 mm from the end of the x-ray optic face and 140 mm from the source. The path difference between x-rays transmitted by the outermost and the central capillaries in our optic corresponds to a temporal broadening of 1.6 ps. This value is comparable with values reported with similar polycapillary x-ray optics.[25,26]

For x-ray detection, we use two different devices. We utilize a commercial megapixel x-ray CCD camera to optimize and monitor the x-ray flux from the plasma source. This CCD is placed next to the x-ray generation chamber and it detects the x-rays coming directly from the water jet that pass through a thin Kapton window on the wall of the chamber and a beryllium window on the entrance face of the CCD. Additionally, the x-rays that pass through the jet, another thin Kapton window, the focusing optic, and sample are analyzed by microcalorimeter array detectors.[27] These direct energy-resolving detectors have been used in predecessor instruments and are described elsewhere.[28]

III. RESULTS

When the femtosecond laser pulse interacts with the water jet, a plasma is generated close to the water surface.[29] The electric field of the driving laser pulse accelerates electrons in the

plasma and x-rays are generated when energetic electrons encounter the water jet. The radiation consists mainly of a Bremsstrahlung continuum and oxygen Kα radiation at 525 eV. The spectra presented here have been corrected for all material transmissions in the x-ray beam path and for the sensitivity and charge redistribution in the CCD as described by Fullagar *et al.*[30] Fig. 2(a) shows the x-ray spectrum from our laser-plasma source as a function of laser pulse energy for a constant laser pulse duration of 35 fs. We can fit the energy region between 6.5 and 11 keV of each spectrum to a simple exponential $N(E) = N_0 \exp(-E/T)$, where N_0, E, and T represent the number of x-ray photons per eV bandwidth per sr per laser pulse, x-ray energy, and electron temperature, respectively. In Fig. 2(b), N_0 is displayed as a function of the laser energy. Additionally, Fig. 2(c) plots the electron temperature for different laser energies. Previous studies have suggested that the hot electron temperature scales as $T \propto (I\lambda^2)^{1/3}$, where I represents the laser intensity and λ the laser wavelength.[31–34] The solid lines in Fig. 2(c)

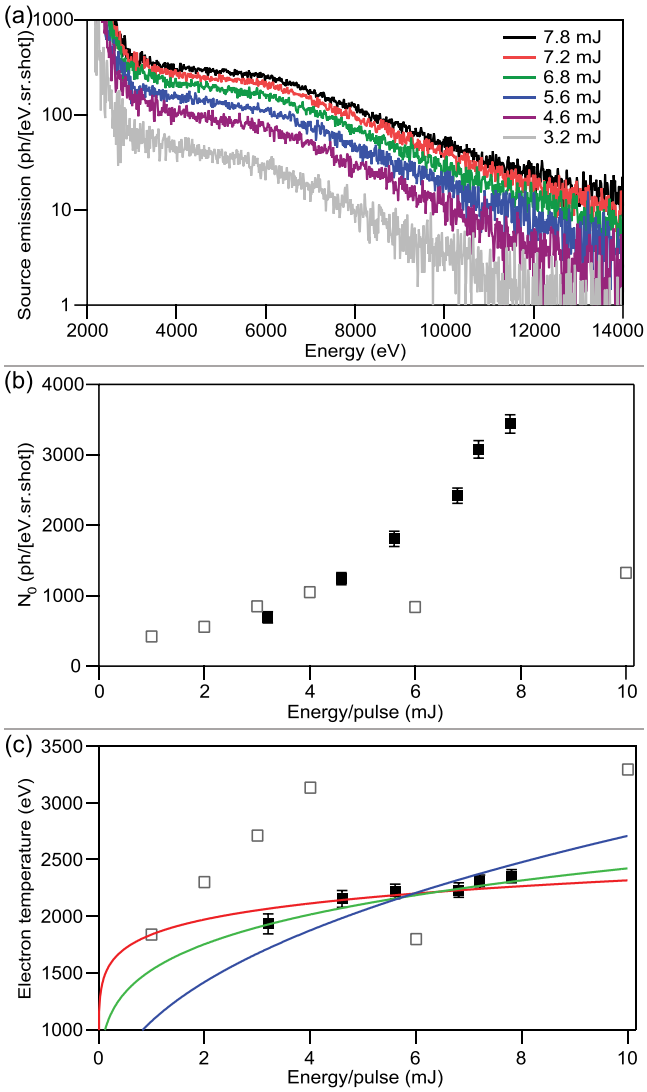

FIG. 2. (a) X-ray spectrum from the water-jet plasma source as a function of laser pulse energy. All spectra have been corrected for the materials transmissions in the x-ray beam path. Between 6.5 and 11 keV, each spectrum can be fitted to a simple exponential $N(E) = N_0 \exp(-E/T)$, where N_0, E, and T represent the number of x-ray photons per eV bandwidth per sr per laser pulse, x-ray energy, and electron temperature, respectively. (b) N_0 as a function of the laser energy. (c) Electron temperature as a function of the laser energy. The solid lines depict a relationship of $T \propto (I\lambda^2)^n$ where I represents the laser intensity, with n taking the values 0.10 (red), 0.29 (green), and 0.40 (blue). In (b) and (c), our data is shown in filled black squares, while data from Fullagar and co-workers is presented in unfilled gray squares.

illustrate a relationship of $T \propto (I\lambda^2)^n$ for different values of n. Our data is well fit by a value of $n = 0.29 \pm 0.03$. Figs. 2(b) and 2(c) also include data obtained by Fullagar *et al.*[30] using a similar x-ray source. Quantitative magnitudes of data from Ref. 30 are in approximate agreement with our results. However, there are significant qualitative differences in the scaling with laser energy per pulse, which are unexplained. These dissimilarities might arise from the different laser systems (e.g., pre-pulse structure) or from environmental variations in the x-ray generation chamber (e.g., base pressure and water vapor).

The shape of the spectra in Fig. 2(a) merits further discussion. The spectra can be divided into three energy regions. At energies below 3 keV, the number of photons diverges unphysically. The divergence is an artifact of the correction for x-ray losses between the source and CCD. Our correction includes 15 μm of Kapton, the 250 μm beryllium window of the CCD, the vendor-supplied CCD efficiency curve, and 8 cm of room air. At low enough energies, the calculated transmission vanishes and the inferred x-ray flux diverges. At energies above 7 keV, the x-ray flux decreases exponentially as a function of x-ray energy. Between 3 and 6 keV, the x-ray flux varies little with x-ray energy. Comparing to previous work, a flat spectral region is absent in some plasma source spectra (water jet,[17,30] aqueous solutions of alkali metal chlorides[19]) but present in others (Cu tape[15] and liquid Hg[21]). This variation in spectral shape among multiple published results raises the question of whether there are physical reasons to expect a flat spectral region. This question has practical importance for absorption spectroscopy with plasma sources since a flat spectral region corresponds to an energy range with suppressed flux compared to simple exponential models. For the 7.8 mJ curve in Fig. 2(a), the measured x-ray flux at 4 keV is reduced by a factor of more than two compared to the value predicted for that energy from the higher energy exponential region of the spectrum. Correctly predicting the shape of the x-ray spectrum is also an important test of theories of x-ray generation from plasma sources.

We therefore set out to test whether a class of models of x-ray generation in plasma sources could account for the flat spectral region between 3 and 6 keV. As mentioned above, the dominant x-ray generation mechanism is expected to be Bremsstrahlung emission produced by energetic electrons within the water jet. For a single laser pulse, the detected x-ray flux at energy E is given by $D(E)\int_{E'>E}^{\infty} f(E')Y(E',E)dE'$ where $D(E)$ is the detection probability at energy E, $f(E')$ is the number of electrons with energy E', and $Y(E',E)$ is the average number of x-rays of energy E generated by electrons with energy E'. We used the software package GEANT4[35,36] to compute $Y(E',E)$ for $E' = 2$, 4, 6, …, and 20 keV; results are shown in Figure 3. GEANT4 is a powerful Monte Carlo simulation package used in nuclear and high energy physics. It includes both electron and photon processes such as, for electrons, multiple scattering, ionization, Bremsstrahlung, and x-ray fluorescence production, and, for photons, photoelectric absorption, Compton scattering, pair production, and Rayleigh scattering. The GEANT4 calculations assume a beam of electrons incident on 1 mm^3 of water of density 1 g/cm^3. The water cube is surrounded by vacuum and by the virtual x-ray collection surface,

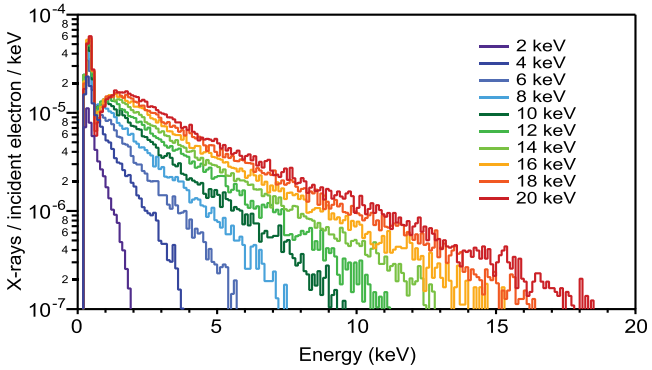

FIG. 3. GEANT4 predictions for the number of x-rays that reach a virtual collection surface surrounding a water target per incident electron per keV. Each curve corresponds to a different initial electron energy E'.

which is a 45 degree cone around the incident axis. At large E, the $Y(E',E)$ curves in Fig. 3 decrease as e^{-E/E_o} where E_o is a characteristic energy that grows with E' so that more energetic electrons produce a harder x-ray spectrum. A strong oxygen Kα emission feature is present at 525 eV. These characteristics are independent of the precise simulation geometry. It can be seen from Fig. 3 that all the calculated x-ray yield curves are decreasing exponentials between 3 and 6 keV while the observed x-ray spectra in Fig. 2(a) are almost flat over this energy range. A logical form for the energy-varying electron number $f(E')$ is Maxwellian.[33] However, given the shape of the x-ray production curves $Y(E',E)$ computed using GEANT4, neither a Maxwellian distribution nor any other simple choice for the electron number distribution $f(E')$ can produce a flat spectrum between 3 and 6 keV. These results potentially exclude a class of models of x-ray generation in plasma sources. In particular, the flat spectral region between 3 and 6 keV observed in Fig. 2(a) is inconsistent with models in which x-ray generation occurs predominantly by the passage of an electron population with a simple energy distribution through a liquid or solid target medium.

We close this discussion of spectral shape with an important caveat. An uncorrected source of x-ray absorption in our CCD measurement could also account for the flat spectral region in Fig. 2(a). However, the amounts of additional beryllium (from the CCD window), Kapton (from the chamber window), or air (from the distance to the CCD) needed to recover an exponential source spectrum cannot be justified. Another possible source of attenuation is water from the jet along the 4 cm path within the x-ray chamber or on the chamber windows. Including the attenuation from an additional 150 μm of water produces a fully exponential spectrum in Fig. 2(a). Is this very significant amount of dispersed water possible? We do not observe water on the Kapton chamber windows and it is unclear whether such a high aerosol concentration can be justified since it would likely scatter the driving laser pulse. However, when the laser is first focused on the water jet, we do observe a decrease in the generated x-ray flux on the timescale of minutes followed by equilibration providing anecdotal evidence that some water is dispersed in the chamber. Quantitative measurements of the dispersed water are needed to fully resolve this question.

We also studied the x-ray yield and electron temperature as a function of the driving laser group delay dispersion with the aim of maximizing the x-ray flux. By changing the distance between the gratings in the pulse compressor of our laser system we can adjust the group delay dispersion, also referred to as laser chirp, in a range of -2000 to $+5600$ fs^2. The laser pulse duration is concomitantly varied from 35 to 500 fs, where a zero-chirp pulse corresponds to a pulse duration of 35 fs. We use a frequency-resolved optical gating (FROG) apparatus to measure the chirp that was introduced in the laser pulses. Fig. 4(a) displays the x-ray yield as a function of laser chirp for a constant laser energy of 7.8 mJ/pulse. Our data shows an increase in the x-ray yield of a factor of three between a positively chirped pulse ($+2135$ fs^2) and an unchirped pulse. Our experimental setup did not allow us to study the effects of a negative chirp pulse over a long range, but we were still able to increase the x-ray yield by a factor of 2.5 in comparison to unchirped pulses. Fig. 4(b) shows the electron temperature as a function of group delay dispersion. Similarly to the x-ray yield, the electron temperature shows two maxima, one at positive and one at negative laser chirp. Overall, the electron temperature and the x-ray yield show a similar behavior as a function of the driving laser group delay dispersion. As proposed by Sohbatzadeh *et al.*[37] and Khachatryan *et al.*,[38] the energy of the plasma electrons can be changed through the interaction with a chirped laser pulse, thus increasing the electron temperature and x-ray yield when these accelerated electrons interact with the water jet. Similar results for the dependence of x-ray yield and spectral hardness on chirp have been presented by Silies for a high-Z target.[39] Similar results for the dependence of x-ray yield on chirp have been presented by Fullagar *et al.* for a low-Z target.[17]

As mentioned previously, we use a polycapillary x-ray optic to image the x-ray source onto the location of our sample jet. Once the x-rays are collected by the optic, the transmission efficiency varies between 8% and 12% for x-rays in the 2–16 keV region. Fig. 5 shows the x-ray spectra, as measured by the CCD camera at the sample position. The chirp was chosen to maximize the x-ray yield. The spectra are corrected for the detection efficiency of the CCD,

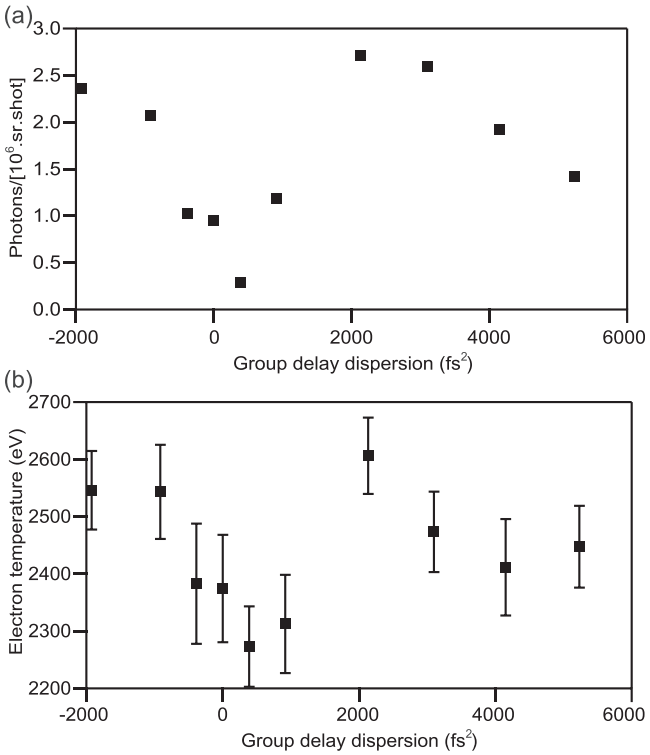

FIG. 4. (a) X-ray yield as a function of group delay dispersion of the driving laser pulse with a constant laser energy of 7.8 mJ. The x-ray yield increased by a factor of three with the introduction of a positive (+2135 fs^2) chirp, which corresponds to a 170 fs pulse. A zero-chirp pulse corresponds to a 35 fs duration. (b) Electron temperature as a function of group delay dispersion. The x-ray yield and electron temperature show a similar behavior as a function of laser chirp.

but not for any materials transmissions between the source and the sample. Integrating over the spectra for the different laser energies yields the total number of photons per second at the sample spot. The measured diameter of the x-ray spot was 75 μm FWHM, in good agreement with the vendor's specification. For our highest laser pulse energy of 7.8 mJ, we obtain an x-ray flux of approximately 4.3×10^6 photons/s.

The application of table-top sources like this one in time-resolved x-ray spectroscopy experiments is dependent on the stability of the x-ray flux and the consistency of the x-ray spectrum. The stability of the x-ray flux relies on multiple factors, i.e., laser beam pointing at the interaction region, energy per pulse of the laser, and spatial stability of the target jet. In order to track these values on a single-pulse basis, we placed three synchronized mechanical choppers in the laser beam path to decrease the repetition rate to 2 Hz, and then we were able to record single-pulse x-ray spectra with the CCD camera for a period of 15 min. The measured

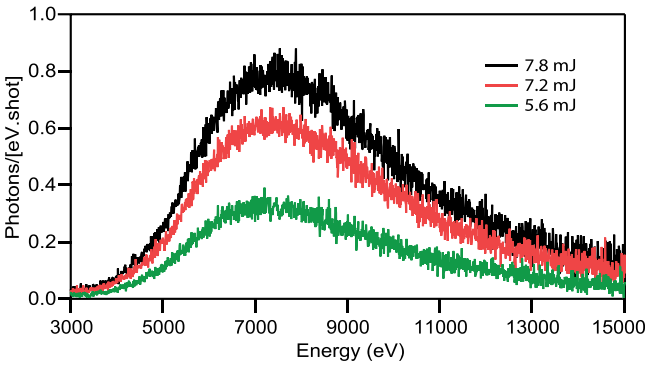

FIG. 5. X-ray spectra at the sample position for different laser pulse energies. The displayed spectra were measured with the CCD camera and are not corrected for attenuation between the source and sample position.

x-ray flux had a pulse-to-pulse standard deviation of ∼8%, where we defined the x-ray flux as the sum of all x-rays present in the CCD camera in a single pulse. We then used a series of diagnostic probes to understand the origins of the flux variation. These diagnostics included simultaneous, pulse-by-pulse monitoring of the laser pulse energy and focus position using a number of pick-offs in the laser beam path.

We assessed two possible causes for the x-ray flux variation: (i) Fluctuations in the laser pulse energy and (ii) movement of the laser focal spot. (i) We used a thermal sensor to measure an average power of 7.85 W at a repetition rate of 1 kHz, resulting in a mean energy per pulse of 7.85 mJ. Additionally, we used a photodiode in its linear regime to determine the standard deviation of the laser energy, obtaining a value of 0.08 mJ. Analyzing our data from Fig. 2, we estimate a decrease in the x-ray flux of 19% per mJ variation in the laser energy. Since the measured standard deviation of the laser energy was 0.08 mJ, we expect the variation in x-ray flux to be 1.5%. (ii) Using a pickoff window immediately before the parabolic mirror, we measured the beam pointing stability of the x-ray generation optical path. This measurement implies a standard deviation of 3 μm for the position of the focused laser spot on the water jet.

We then measured the changes in the x-ray flux as we varied the spatial overlap between the laser pulse and the target jet. First, we maximized the x-ray flux by optimizing the interaction region between the laser and the water jet. The x-ray flux was maximized when the laser was focused at the edge of the jet. We then moved the laser beam 10 μm into the water jet, resulting in a decrease of 20% in the x-ray flux. Finally, we moved 10 μm away from the water jet, which produced a 50% decrease of the x-ray flux. Knowing the linearized change in flux per micrometer displacement and the range of deviation for both the target jet and the laser pointing we were able to calculate the expected variation of the x-ray flux due to the measured motion of the laser beam jet. Using a 3 μm displacement in the laser pointing, we calculate a 7.8% standard deviation in the x-ray flux.

If we add these two sources of variation in quadrature, we compute the standard deviation of the x-ray flux to be ∼7.9% which is similar to the measured value of 8.1%. From our measurements, it appears that the laser pointing instability is the main source of instability in the x-ray yield. The path length on the optical table between the laser and target chamber is 4.5 m and includes multiple optical elements, all of which in addition to the laser itself can contribute to the pointing instability.

On timescales of hours, we often observe a decrease in the x-ray flux of 10%–30%. We believe these large flux changes are also due to instability of the laser pointing. We ruled out changes in the water jet on these timescales by photographing the target jet every 10 min over a period of 8 h. Over the course of these measurements we observed maximum side-to-side movement of the jet of only 2–3 μm. The peak x-ray flux value can be restored easily by translating the water jet chamber along the direction of motion perpendicular to the incident laser beam. Presently, these translations are performed manually but an automatic feedback circuit that seeks to maintain the x-ray flux observed by the CCD could be used to make these adjustments automatically in the future. We note that the position and orientation of the x-ray optic is fixed relative to the chamber so that movements of the chamber to re-locate the laser focus relative to the water jet do not disrupt the alignment of the optic to the point of x-ray generation. During a time-resolved experiment, the area of excitation of the pump is chosen to be large enough to make the influence of these movements on the output x-ray spot negligible.

The number of x-ray photons that reach the microcalorimeter array from a single laser pulse is 10–100, which is at least seven orders of magnitude smaller than the number of x-rays required to generate a high quality absorption spectrum with our apparatus. Hence, x-ray measurements from 10^7 or more laser pulses must be summed. It is therefore necessary to confirm that the spectral distribution that describes the output of the plasma source does not vary from pulse to pulse. As described above, we used an x-ray CCD camera to acquire a series of single-pulse x-ray spectra. One such single-pulse spectrum, without correction for any material transmission, along with the average spectrum from 444 pulses is shown in the inset of Figure 6. While the single pulse spectrum superficially resembles the average result, many of the energy bins are empty in the single pulse measurement, complicating rigorous comparison. In the main

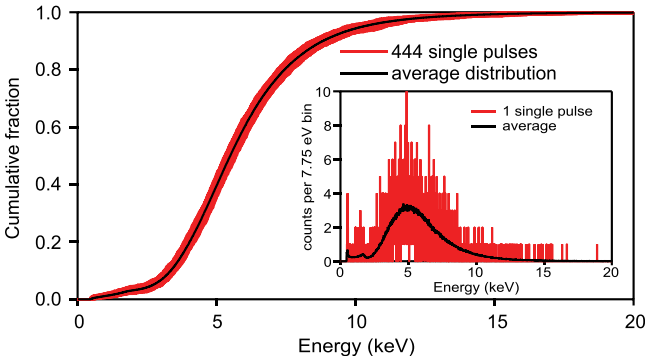

FIG. 6. Plotted in the inset is the measured x-ray spectrum from a single laser pulse (red) and the average of 444 pulses (black). The x-ray flux is peaked near 5 keV and decays exponentially at higher energies. Plotted in the main figure is the CFF of the average spectrum (black). Shown in red are the CFFs of the 444 individual pulse spectra. They can be seen to closely resemble the average CFF.

panel of Figure 6, we show the Cumulative Fraction Function (CFF)[40] of the average spectrum in black. The CFF is the Cumulative Distribution Function normalized to unity. Hence, the energy-varying CFF(E) for an x-ray spectrum describes the fraction of the x-rays present in the spectrum below energy E. The CFF provides a powerful means of visualizing the shape of sparse spectra. The CFFs of the 444 single pulse spectra are shown in red and form a band around the average result. The largest difference between any single CFF and the average CFF at any energy is 0.052 and the typical difference is considerably smaller. Hence, we have confirmed that the pulse-to-pulse spectral variation of our laser plasma source is negligible.

As previously mentioned, the goal of this setup is to perform time-resolved XAS experiments. Fig. 7 shows a static x-ray absorption spectrum of an ammonium ferrioxalate/water

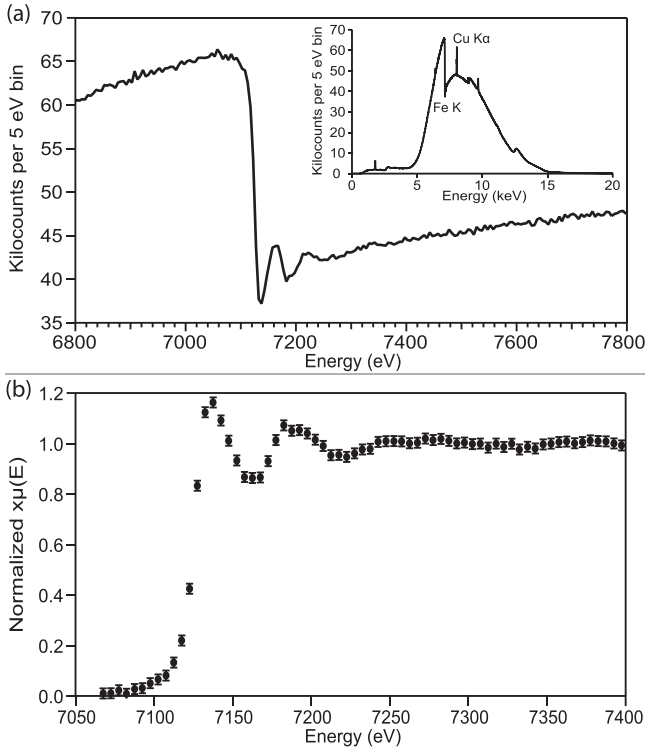

FIG. 7. (a) Laser plasma absorption spectrum of ferrioxalate in transmission mode around the Fe K-edge displayed as measured number of x-rays versus x-ray energy. The inset shows the entire energy range recorded with an array of microcalorimeter detectors. The measured spectrum contains emission lines from copper metal located beneath the detectors. (b) Normalized absorption spectrum of ferrioxalate showing EXAFS features.

solution. Ferrioxalate has been intensely studied with optical and x-ray spectroscopy[41–43] since it is used as a chemical actinometer and it is responsible for oxygen consumption in natural waters.[44] We used a gear pump to recirculate the ferrioxalate solution within a contained circuit broken by a free-space jet defined by an aperture consisting of a linear array of four 100 μm diameter holes on a 150 μm pitch. The x-ray beam travels along the axis of the array of four circular jets in order to increase the interaction of the x-rays with the sample. Fig. 7(a) shows the x-ray absorption fine-structure spectrum of 1.2 M ferrioxalate in water collected with the microcalorimeter detector array. In addition to the Fe K-edge and absorption fine-structure features, the measured spectrum contains emission lines from copper metal located beneath the detectors. Fig. 7(b) shows the normalized absorption spectrum of the ferrioxalate sample. The error bars for each bin were obtained from the Poisson error of the recorded number of photons per bin in Fig. 7(a). In upcoming work, we compare static absorption measurements to measurements performed at a synchrotron, to theoretical calculations, and to absorption measurements acquired after photoexcitation of the sample.

IV. CONCLUSION

We have presented an x-ray plasma source for ultrafast x-ray absorption spectroscopy. The plasma source is driven by a commercially available Ti:Sapphire laser system that interacts with a water jet to produce sub-picosecond x-ray pulses with a broad energy distribution from 2–15 keV. We explored the variations in the x-ray flux as a function of laser pulse energy and duration. We examined the spectral shape of our spectra and compared it with spectra simulated with the software package GEANT4. We performed single-pulse measurements to study source stability, both in terms of x-ray flux and x-ray spectral shape. Finally, we showed a static x-ray absorption spectrum of a ferrioxalate/water solution. Our results demonstrate that the described plasma source is a suitable candidate for laboratory-based time-resolved x-ray absorption spectroscopy experiments.

ACKNOWLEDGMENTS

This work was supported by the NIST Innovations in Measurement Science Program. J. Uhlig gratefully acknowledges the continued funding from the Knut and Alice Wallenberg Foundation.

[1]A. Rousse, C. Rischel, and J. Gauthier, "Colloquium: Femtosecond x-ray crystallography," Rev. Mod. Phys. **73**, 17 (2001).
[2]L. X. Chen, W. J. Jäger, G. Jennings, D. J. Gosztola, A. Munkholm, and J. P. Hessler, "Capturing a photoexcited molecular structure through time-domain x-ray absorption fine structure," Science **292**, 262 (2001).
[3]M. Bargheer, N. Zhavoronkov, M. Woerner, and T. Elsaesser, "Recent progress in ultrafast X-ray diffraction," Chemphyschem **7**, 783 (2006).
[4]R. W. Schoenlein, "Generation of femtosecond pulses of synchrotron radiation," Science **287**, 2237 (2000).
[5]S. Khan, K. Holldack, T. Kachel, R. Mitzner, and T. Quast, "Femtosecond undulator radiation from sliced electron bunches," Phys. Rev. Lett. **97**, 074801 (2006).
[6]P. Beaud, S. Johnson, A. Streun, R. Abela, D. Abramsohn, D. Grolimund, F. Krasniqi, T. Schmidt, V. Schlott, and G. Ingold, "Spatiotemporal stability of a femtosecond hard–x-ray undulator source studied by control of coherent optical phonons," Phys. Rev. Lett. **99**, 174801 (2007).
[7]B. W. J. McNeil and N. R. Thompson, "X-ray free-electron lasers," Nat. Photonics **4**, 814 (2010).
[8]F. Ráksi, K. R. Wilson, Z. Jiang, A. Ikhlef, C. Y. Coté, and J.-C. Kieffer, "Ultrafast x-ray absorption probing of a chemical reaction," J. Chem. Phys. **104**, 6066 (1996).
[9]T. Lee, Y. Jiang, C. G. Rose-Petruck, and F. Benesch, "Ultrafast tabletop laser-pump-x-ray probe measurement of solvated $Fe(CN)_6^{4-}$," J. Chem. Phys. **122**, 84506 (2005).
[10]J. Chen, H. Zhang, I. V. Tomov, X. Ding, and P. M. Rentzepis, "Electron transfer and dissociation mechanism of ferrioxalate: A time resolved optical and EXAFS study," Chem. Phys. Lett. **437**, 50 (2007).
[11]C. Rose-Petruck, R. Jimenez, and T. Guo, "Picosecond-milliangström lattice dynamics measured by ultrafast X-ray diffraction," Nature **398**, 310 (1999).
[12]N. Zhavoronkov, Y. Gritsai, M. Bargheer, M. Woerner, T. Elsaesser, F. Zamponi, I. Uschmann, and E. Förster, "Microfocus Cu K(alpha) source for femtosecond x-ray science.," Opt. Lett. **30**, 1737 (2005).
[13]Y. Jiang, T. Lee, W. Li, G. Ketwaroo, and C. G. Rose-Petruck, "High-average-power 2-kHz laser for generation of ultrashort x-ray pulses," Opt. Lett. **27**, 963 (2002).
[14]E. Fill, J. Bayerl, and R. Tommasini, "A novel tape target for use with repetitively pulsed lasers," Rev. Sci. Instrum. **73**, 2190 (2002).

[15]F. Zamponi, Z. Ansari, C. K. Schmising, P. Rothhardt, N. Zhavoronkov, M. Woerner, T. Elsaesser, M. Bargheer, T. Trobitzsch-Ryll, and M. Haschke, "Femtosecond hard X-ray plasma sources with a kilohertz repetition rate," Appl. Phys. A **96**, 51 (2009).
[16]M. Silies, H. Witte, S. Linden, J. Kutzner, I. Uschmann, E. Förster, and H. Zacharias, "Table-top kHz hard X-ray source with ultrashort pulse duration for time-resolved X-ray diffraction," Appl. Phys. A **96**, 59 (2009).
[17]W. Fullagar, M. Harbst, S. Canton, J. Uhlig, M. Walczak, C.-G. Wahlström, and V. Sundström, "A broadband laser plasma x-ray source for application in ultrafast chemical structure dynamics," Rev. Sci. Instrum. **78**, 115105 (2007).
[18]R. J. Tompkins, I. P. Mercer, M. Fettweis, C. J. Barnett, D. R. Klug, L. G. Porter, I. Clark, S. Jackson, P. Matousek, A. W. Parker, and M. Towrie, "5–20 keV laser-induced x-ray generation at 1 kHz from a liquid-jet target," Rev. Sci. Instrum. **69**, 3113 (1998).
[19]K. Hatanaka, T. Miura, and H. Fukumura, "Ultrafast x-ray pulse generation by focusing femtosecond infrared laser pulses onto aqueous solutions of alkali metal chloride," Appl. Phys. Lett. **80**, 3925 (2002).
[20]G. Korn, A. Thoss, H. Stiel, U. Vogt, M. Richardson, T. Elsaesser, and M. Faubel, "Ultrashort 1-kHz laser plasma hard x-ray source," Opt. Lett. **27**, 866 (2002).
[21]C. Reich, C. M. Laperle, X. Li, B. Ahr, F. Benesch, and C. G. Rose-Petruck, "Ultrafast x-ray pulses emitted from a liquid mercury laser target.," Opt. Lett. **32**, 427 (2007).
[22]J. Uhlig, C.-G. Wahlström, M. Walczak, V. Sundström, and W. Fullagar, "Laser generated 300 keV electron beams from water," Laser Part. Beams **29**, 415 (2011).
[23]M. Bargheer, N. Zhavoronkov, R. Bruch, H. Legall, H. Stiel, M. Woerner, and T. Elsaesser, "Comparison of focusing optics for femtosecond X-ray diffraction," Appl. Phys. B **80**, 715 (2005).
[24]U. Shymanovich, M. Nicoul, K. Sokolowski-Tinten, A. Tarasevitch, C. Michaelsen, and D. von der Linde, "Characterization and comparison of X-ray focusing optics for ultrafast X-ray diffraction experiments," Appl. Phys. B **92**, 493 (2008).
[25]I. V. Tomov, J. Chen, X. Ding, and P. M. Rentzepis, "Efficient focusing of hard X-rays generated by femtosecond laser driven plasma," Chem. Phys. Lett. **389**, 363 (2004).
[26]R. Tommasini, R. Bruch, E. Fill, and A. Bjeoumikhov, "Convergent-beam diffraction of ultra-short hard X-ray pulses focused by a capillary lens," Appl. Phys. B **82**, 519 (2006).
[27]J. N. Ullom, J. A. Beall, W. B. Doriese, W. D. Duncan, L. Ferreira, G. C. Hilton, K. D. Irwin, C. D. Reintsema, and L. R. Vale, "Optimized transition-edge x-ray microcalorimeter with 2.4 eV energy resolution at 5.9 keV," Appl. Phys. Lett. **87**, 194103 (2005).
[28]J. Uhlig, W. Fullagar, J. N. Ullom, W. B. Doriese, J. W. Fowler, D. S. Swetz, N. Gador, S. E. Canton, K. Kinnunen, I. J. Maasilta, C. D. Reintsema, D. A. Bennett, L. R. Vale, G. C. Hilton, K. D. Irwin, D. R. Schmidt, and V. Sundström, "Table-top ultrafast x-ray microcalorimeter spectrometry for molecular structure," Phys. Rev. Lett. **110**, 138302 (2013).
[29]P. Gibbon and A. R. Bell, "Collisionless absorption in sharp-edged plasmas," Phys. Rev. Lett. **68**, 1535 (1992).
[30]W. Fullagar, J. Uhlig, M. Walczak, S. Canton, and V. Sundström, "The use and characterization of a backilluminated charge-coupled device in investigations of pulsed x-ray and radiation sources," Rev. Sci. Instrum. **79**, 103302 (2008).
[31]F. N. Beg, A. R. Bell, A. E. Dangor, C. N. Danson, A. P. Fews, and M. E. Glinsky, "A study of picosecond laser–solid interactions up to 10^{19} W cm^{-2}," Phys. Plasmas **4**, 447 (1997).
[32]J. Yu, Z. Jiang, J. C. Kieffer, and A. Krol, "Hard x-ray emission in high intensity femtosecond laser–target interaction," Phys. Plasmas **6**, 1318 (1999).
[33]C. Reich, P. Gibbon, I. Uschmann, and E. Forster, "Yield optimization and time structure of femtosecond laser plasma k-alpha sources," Phys. Rev. Lett. **84**, 4846 (2000).
[34]J. C. Kieffer, A. Krol, Z. Jiang, C. C. Chamberlain, E. Scalzetti, and Z. Ichalalene, "Future of laser-based X-ray sources for medical imaging," Appl. Phys. B **74**, s75 (2002).
[35]S. Agostinelli, J. Allison, K. Amako, J. Apostolakis, H. Araujo, P. Arce, M. Asai, D. Axen, S. Banerjee, G. Barrand, F. Behner, L. Bellagamba, J. Boudreau, L. Broglia, A. Brunengo, H. Burkhardt, S. Chauvie, J. Chuma, R. Chytracek, G. Cooperman, G. Cosmo, P. Degtyarenko, A. Dell'Acqua, G. Depaola, D. Dietrich, R. Enami, A. Feliciello, C. Ferguson, H. Fesefeldt, G. Folger, F. Foppiano, A. Forti, S. Garelli, S. Giani, R. Giannitrapani, D. Gibin, J. J. Gómez Cadenas, I. González, G. Gracia Abril, G. Greeniaus, W. Greiner, V. Grichine, A. Grossheim, S. Guatelli, P. Gumplinger, R. Hamatsu, K. Hashimoto, H. Hasui, A. Heikkinen, A. Howard, V. Ivanchenko, A. Johnson, F. W. Jones, J. Kallenbach, N. Kanaya, M. Kawabata, Y. Kawabata, M. Kawaguti, S. Kelner, P. Kent, A. Kimura, T. Kodama, R. Kokoulin, M. Kossov, H. Kurashige, E. Lamanna, T. Lampén, V. Lara, V. Lefebure, F. Lei, M. Liendl, W. Lockman, F. Longo, S. Magni, M. Maire, E. Medernach, K. Minamimoto, P. Mora de Freitas, Y. Morita, K. Murakami, M. Nagamatu, R. Nartallo, P. Nieminen, T. Nishimura, K. Ohtsubo, M. Okamura, S. O'Neale, Y. Oohata, K. Paech, J. Perl, A. Pfeiffer, M. G. Pia, F. Ranjard, A. Rybin, S. Sadilov, E. Di Salvo, G. Santin, T. Sasaki, N. Savvas, Y. Sawada, S. Scherer, S. Sei, V. Sirotenko, D. Smith, N. Starkov, H. Stoecker, J. Sulkimo, M. Takahata, S. Tanaka, E. Tcherniaev, E. Safai Tehrani, M. Tropeano, P. Truscott, H. Uno, L. Urban, P. Urban, M. Verderi, A. Walkden, W. Wander, H. Weber, J. P. Wellisch, T. Wenaus, D. C. Williams, D. Wright, T. Yamada, H. Yoshida, and D. Zschiesche, "Geant4—a simulation toolkit," Nucl. Instrum. Methods Phys. Res., Sect. A **506**, 250 (2003).
[36]J. Allison, K. Amako, J. Apostolakis, H. Araujo, P. A. Dubois, M. Asai, G. Barrand, R. Capra, S. Chauvie, R. Chytracek, G. A. P. Cirrone, G. Cooperman, G. Cosmo, G. Cuttone, G. G. Daquino, M. Donszelmann, M. Dressel, G. Folger, F. Foppiano, J. Generowicz, V. Grichine, S. Guatelli, P. Gumplinger, A. Heikkinen, I. Hrivnacova, A. Howard, S. Incerti, V. Ivanchenko, T. Johnson, F. Jones, T. Koi, R. Kokoulin, M. Kossov, H. Kurashige, V. Lara, S. Larsson, F. Lei, O. Link, F. Longo, M. Maire, A. Mantero, B. Mascialino, I. Mclaren, P. M. Lorenzo, K. Minamimoto, K. Murakami, P. Nieminen, L. Pandola, S. Parlati, L. Peralta, J. Perl, A. Pfeiffer, M. G. Pia, A. Ribon, P. Rodrigues, G. Russo, S. Sadilov, G. Santin, T. Sasaki, D. Smith, N. Starkov, S. Tanaka, E. Tcherniaev, B. Tomé, A. Trindade, P. Truscott, L. Urban, M. Verderi, A. Walkden, J. P. Wellisch, D. C. Williams, D. Wright, and H. Yoshida, "Geant4 developments and applications," IEEE Trans. Electron Devices **53**, 270 (2006).
[37]F. Sohbatzadeh, S. Mirzanejhad, and M. Ghasemi, "Electron acceleration by a chirped Gaussian laser pulse in vacuum," Phys. Plasmas **13**, 123108 (2006).

[38]A. Khachatryan, F. van Goor, and K.-J. Boller, "Interaction of free charged particles with a chirped electromagnetic pulse," Phys. Rev. E **70**, 067601 (2004).
[39]M. Silies, S. Linden, H. Witte, and H. Zacharias, "The dependence of the Fe K α yield on the chirp of the femtosecond exciting laser pulse," Appl. Phys. B **87**, 623 (2007).
[40]W. H. Press, S. A. Teukolsky, W. T. Vetterling, and B. P. Flannery, *Numerical Recipes: The Art of Scientific Computing*, 3rd ed. (Cambridge University Press, 2007).
[41]J. Chen, H. Zhang, I. V. Tomov, M. Wolfsberg, X. Ding, and P. M. Rentzepis, "Transient structures and kinetics of the ferrioxalate redox reaction studied by time-resolved EXAFS, optical spectroscopy, and DFT," J. Phys. Chem. A **111**, 9326 (2007).
[42]I. P. Pozdnyakov, O. V. Kel, V. F. Plyusnin, V. P. Grivin, and N. M. Bazhin, "New insight into photochemistry of ferrioxalate," J. Phys. Chem. A **112**, 8316 (2008).
[43]Y. Obara, T. Katayama, Y. Ogi, T. Suzuki, N. Kurahashi, S. Karashima, Y. Chiba, Y. Isokawa, T. Togashi, Y. Inubushi, M. Yabashi, T. Suzuki, and K. Misawa, "Femtosecond time-resolved X-ray absorption spectroscopy of liquid using a hard X-ray free electron laser in a dual-beam dispersive detection method," Opt. Express **22**, 1105 (2014).
[44]C. J. Miles and P. L. Brezonik, "Oxygen consumption in humic-colored waters by a photochemical ferrous-ferric catalytic cycle," Environ. Sci. Technol. **15**, 1089 (1981).
[45]J. Weisshaupt, V. Juvé, M. Holtz, S. Ku, M. Woerner, T. Elsaesser, S. Ališauskas, A. Pugžlys, and A. Baltuška, "High-brightness table-top hard x-ray source driven by source driven by sub-100-femtosecond mid-infrared pulses," Nature Photonics **8**, 927 (2014).